The Bordeaux "Pont de Pierre" – A study case of micropiles reinforcement and benefits of HST method and Interaction Soil Structure design

G Valdeyron, Stéphane Bonelli, P Losset, M Mariko

Geotechnical Engineering for the Preservation of Monuments and Historic Sites III – Lancellotta, Viggiani, Flora, de Silva & Mele (Eds)

The Bordeaux "Pont de Pierre" – A study case of micropiles reinforcement and benefits of HST method and Interaction Soil Structure design

G. Valdeyron
Cerema, Bordeaux, France

S. Bonelli
RECOVER, INRAE and Aix-Marseille Univ., Aix-en-Provence, France

P. Losset
Cerema, Bordeaux, France

M. Mariko
Bordeaux-Métropole, Bordeaux, France

ABSTRACT: The "Pont de Pierre" of Bordeaux (France), built between 1810 and 1821, was, until 2014, the only link between the two borders of the Garonne River. Today, it is a strategical axis that is used every day by 100 000 passengers (on foot, by bicycle or by tram). Since its construction, the bridge has been affected by significant settlement. In 1992–1994 and 2002–2003, 16 micropiles drilled into the masonry of each pillar reinforced the first six pillars. A detailed monitoring analysis (before and after reinforcement) is undertaken to expose the effects of micropile reinforcement and the load transfer process. In addition, an analysis of tidal effects is also carried out. Then, a soil-structure interaction model and a soil-pile-soil model are developed and fitted to the previous analysis. The results are compared with the reinforcement design obtained by the safety factor approach. The importance of considering the relative stiffness between micropiles and timber piles to improve the design of reinforcements (micropiles) is highlighted. The analysis sheds light on the issue of strengthening the last 11 pillars projected for 2023–2025.

1 HISTORICAL BACKGROUND, GEOTECHNICAL AND STRUCTURAL ASPECTS

1.1 *Bridge design, history of the building*

The "Pont de Pierre" bridge was the first to be built over the Garonne in Bordeaux. Its construction, under the responsibility of the engineer Deschamps, began in 1812. The following year, 8 of the first 11 piers built were destroyed by a flood. Considerations of redesign and financial difficulties delayed construction and the bridge was completed in 1821.

The Stone Bridge is 486 m long and consists of 16 low masonry arches with an average span of 23 m. Due to the poor properties of the foundation soil, the bridge is founded on wooden piles anchored in more or less compacted coarse sand. In addition, each pier is lightened by two levels of arches that replace the backfill material (see Figure 1).

In order to limit the weight, but also the financial cost of the structure, the designers decided to use two kinds of mineral resources. The voussoirs of the arch quoins are made of hard limestone ashlars. Between them, the rest of the arches are made of bricks made of silty clay taken directly from the Garonne.

 DOI 10.1201/9781003308867-56

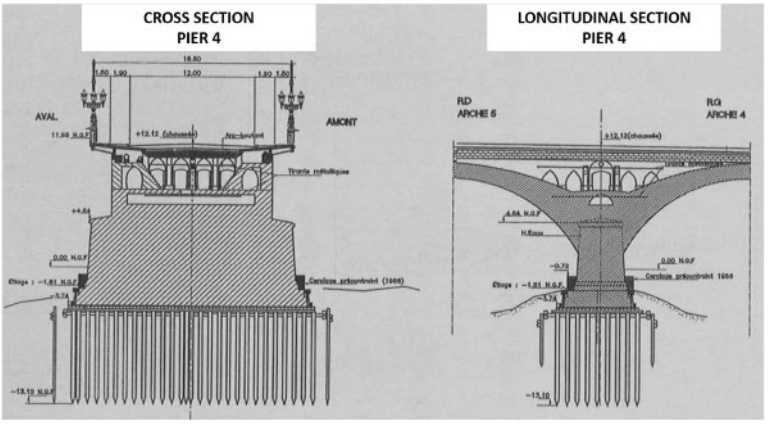

Figure 1. Transversal and elevation cut of a pier.

Each pile rests on a foundation of approximately 250 driven wooden piles, all of which are connected by a wooden deck. The latter was initially built on the banks of the Garonne and topped with the first three rows of masonry, at the edge, some sort of walls were built in order to turn it into a boat, which was beached on the group of piles.

The edge of each pillar is covered with rockfill to provide protection against scouring. The protection of the bridge against scouring was one of the main concerns of the designers, as Claude Deschamps sums up: "This monument will remain standing as long as the engineers take care of the rockfill protection". Indeed, the rockfill was backfilled in 1901, 1928, 1939, 1967, 1987, 1993, 1995–1997, 2018, however, as can be seen in Figure 2, the sub-river slopes remain a major problem, and are deeper than the pile ends.

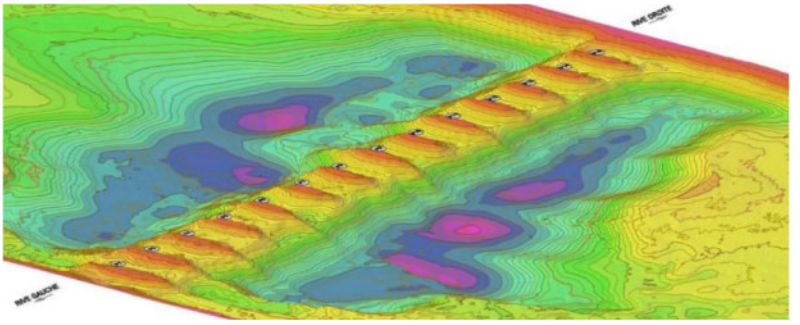

Figure 2. Bathymetry.

Since the beginning of construction, the bridge has been affected by excessive settlement, the left edge piers were the first to be affected, and for example, a through fracture of about 12 mm occurred on the second pier and required post-tensioning (400 kN) around it in 1899. The same process was applied to Pile 1 (1910) and Piles 3 and 4 (1994). It appears that, since the beginning of construction, settlements continue over the years.

1.2 *Geological and geotechnical aspects*

From top to bottom, recent alluvial deposits make up the foundation soil, overlying the Oligocene marl and limestone which form the geotechnical substrate of the bridge foundation. Muddy clays, silty sands, sands and gravels composed of recent alluvium. From the left edge to the right (pier 1

to 16), the alluvial layer becomes thinner and less clayey. The geotechnical properties of the soil are summarized in the longitudinal profile (see Figure 3).

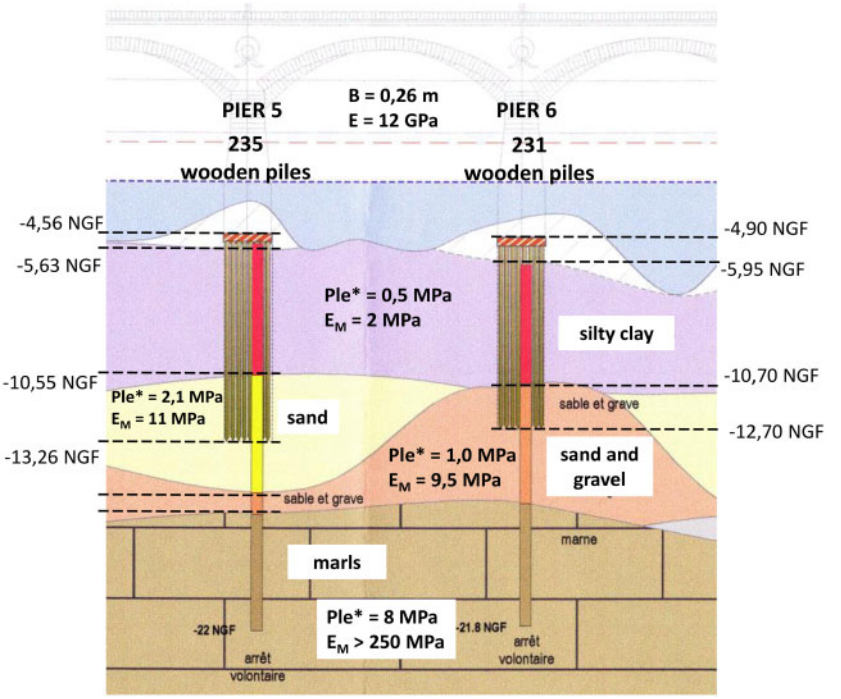

Figure 3. Longitudinal profile.

Soil strength is mainly studied using the Menard Pressumeter Test (PMT) and laboratory tests (oedometer and triaxial tests). The alluvium has poor mechanical characteristics and high compressibility ($Pl_e^* = 0.5$ MPa – $2 < E_M < 4$ MPa, $1.2 < Cc < 1.7$). The sands and gravels have higher characteristics (1 MPa $< Pl_e^* <$ 2.1 MPa – $15 < E_M < 30$ MPa).

The bridge is subject to tidal cycles of about 12:25, so every day there are two high and low tides. This implies a cyclic action on the foundation of the pile group, due to flotation, of about 5 m, or, which is equivalent, a 10% variation of the load on the pile group.

In addition, a controlled static compression load test was performed on a test micropile to evaluate the load displacement behavior of the pile and the surrounding soil (stiffness $K_{\mu p} = 100\,000$ kN/m) and the limiting friction of the shaft in the marls ($q_s > 750$ kPa).

1.3 *Monitoring implementation and structural behaviour*

The settlements of the bridge have been measured since 1992 by a fixed point system installed on each pier and consisting of a micropile anchored (6 m) in the marl (fixed point) and sealed in the masonry pier. Free movement in the alluvium is provided by a larger diameter pipe that surrounds the hole. In addition, a clinometer is installed on each pier to measure the upstream/downstream inclination.

Between 1991 and 2002, the settlements were measured with a variable measurement time step (1 measurement per half hour to 1 measurement/3 hours). A new monitoring system, implemented in 2003, increases the time step to one measurement per hour. The accuracy of the settlement gauges is 1/1000 mm.

Tide levels are measured by tide gauges located 4 km downstream from the bridge. The phase shift between the tide gauge measurements and the water level at the bridge is neglected.

2 THE HYDROSTATIC-SEASON-TIME (HST) MODEL

The tools most commonly used for dam monitoring data analysis purposes are the statistical methods of the Hydrostatic-Season-Time (HST) type. These methods were first developed in the 1960s to analyze the displacements resulting from the pendulum effects occurring at arch dams (Ferry & Willm 1958). They are still being used in several countries to analyze measurements of other kinds (Bonelli 2008, 2009; Carrère et al. 2000; Guedes & Coehlo 1985).

The HST model is based on effects of three kinds. First there are the hydrostatic effects, which correspond to the variations H resulting from changes in the water level. This variable is given by a polynomial of order 4 (parameters a_1, a_2, a_3, a_4):

$$H(t) = a_1 z(t) + a_2 z^2(t) + a_3 z^3(t) + a_4 z^4(t) \tag{1}$$

with $z(t) = (Z(t) - Z_{min})/(Z_{max} - Z_{min})$, where $Z(t)$ is the reservoir level (minimum value Z_{min}, maximum value Z_{max}).

The second term is the time of year, which accounts for seasonal variations S in the measurements during twelve-month and six-month periods, is described by the following expression (parameters A_1, d_1, A_2, d_2):

$$S(t) = A_1 sin(\omega_a(t - d_1)) + A_2 sin(2\omega_a(t - d_2)) \tag{2}$$

where $\omega_a = 2\pi/T_a$ is the annual angular frequency (T_a corresponds to a one-year period). The seasonal variations effect, assumed to be reversible, is quantified by maximum amplitudes A_i and lag time d_i. One of the oldest known application of this model was developed by Forbes (1846) who used the so called "sinusoidal adjustment method" to account for cyclic variations in the ground temperature.

The third term accounts for the time-dependent trends in the ageing processes. This variable is often called the "irreversible effect". It is expressed as follows (parameters c_1, c_2, c_3):

$$T(t) = c_1 \tau + c_2 exp(\tau) + c_3 exp(\tau) \tag{3}$$

with $\tau = (t - t_0)/\Delta T$, where t is time, and $[t_0, t_0 + \Delta T]$ is the analysis interval. The settlement rate is given by the time derivative, estimated in the middle of the analysis interval:

$$v_1 = [c_1 + c_2 exp(1/2) - c_3 exp(-1/2)]/\Delta T \tag{4}$$

The HST model $Y(t) = Y_0 + H(t) + S(t) + T(t)$ has 11 parameters estimated by multiple linear regression with MSE $||y - Y||^2$ where y is the measurement. This approach has been classically used to analyze dam monitoring data. The experience acquired at several hundreds of dams has confirmed what an excellent tool this approach can be for interpreting monitoring data. It has also been used in many other fields (Young 1998). In the present work, the HST model is applied to vertical displacement analysis measured on the Pont de Pierre.

3 APPLICATION AND RESULTS OF THE HST METHOD TO THE PONT DE PIERRE

The analysis is based on two time intervals:

- before the reinforcement work, between 1992 and 1993 (for P01 to P04) and 1992 and 2002 (for P05 to P16), i.e. 10 years (115 measurements);
- after the reinforcement works, between 2003 and 2021, i.e. 19 years (145,000 measurements).

The results are detailed for pier P06 in Figure 4 (before reinforcement works) and Figure 5 (after reinforcement works). Before reinforcement works, the reversible displacements due to buoyancy (Figure 4a) and outdoor temperature (Figure 4b) are two orders of magnitude smaller than the creep settlement (Figure 4c), which is linear in time. After the reinforcement works, the reversible

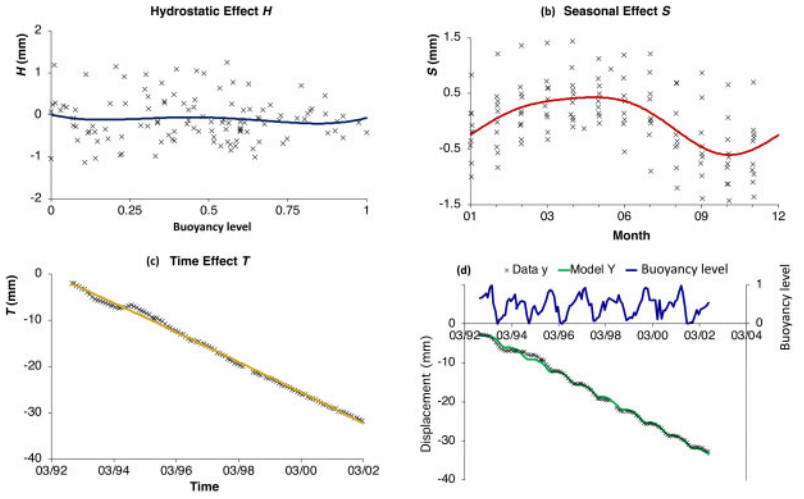

Figure 4. Results of HST analysis of P06 measurements on 1992–2002 time interval (before reinforcement): (a) Hydrostatic effect H, (b) Seasonal effect S, (c) Time effect T, (d) Data, Model and Buoyancy level as a function of time.

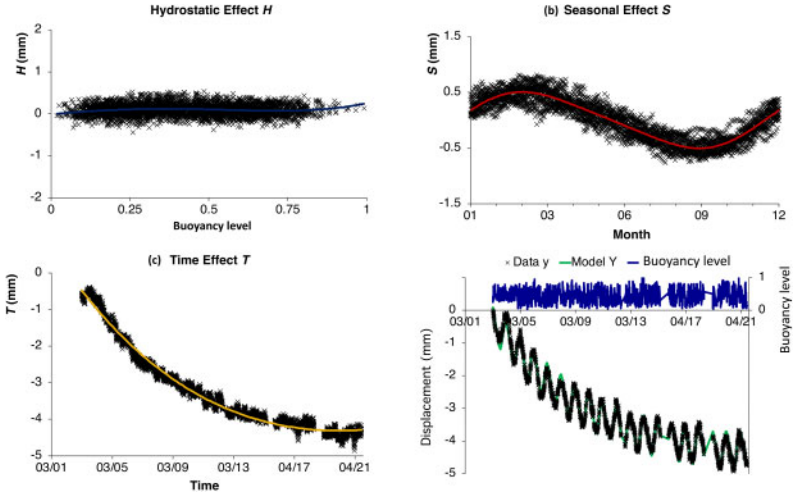

Figure 5. Results of HST analysis of P06 measurements on 2003–2021 time interval (after reinforcement): (a) hydrostatic effect H, (b) seasonal effect S, (c) time effect T, (d) data, model and buoyancy level as a function of time.

displacements due to buoyancy remain of very small amplitude (Figure 5a). The magnitudes of reversible displacements due to temperature variations were not changed by the reinforcement work (Figure 5b). On the other hand, it appears that creep settlements are damped and stabilize with time (Figure 5c). Figures 4d and 5d show that the HST analysis accurately reflects the pre- and post-reinforcement measurements.

All HST analyses on the 18 instruments are summarized in Figure 6. The amplitudes of the reversible displacements due to the variations of outside temperature, as well as their phase shift in time, were not modified by the reinforcement works (Figure 6a and 6b). Figure 6d shows that the decrease in creep settlements resulting from the reinforcement work on piers P01 through P06 is shown in Figure 6c. For the reinforced piers (P01-P06), the creep settlements represented 40%

Figure 6. Results of HST analysis of 18 time series on two time interval (before and after reinforcement): (a) amplitude of reversible displacements A_1, (b) lag time d_1, (c) settlement velocity v_1, (d) settlement/total displacement ratio.

to 80% of the total displacements before the works, and about 20% after the works (knowing that the creep displacements stabilize with time). For the unreinforced piers (P07-P16), the creep settlements are about 80% of the total displacements.

4 DESIGN OF THE MICROPILE REINFORCEMENT

4.1 *Safety factor approach*

The excessive settlements observed could be explained by a defect in the bearing capacity of the wood pile group. The bearing capacity is evaluated according to the theory of the pressumeter in relation to the French standard (NF P94-262), and the group effect is evaluated with the Converse-Labarre formulas, which give the effectiveness of the grouping of piles. In our case, the reduction factor is equal to 0.67. According to French practice (Christin 2013), the achieved value of the global safety factor for quasi-permanent SLS for a wood pile foundation is 2.16. Table 1 summarizes the results of the calculations for P01-P06 in terms of the global safety factor approach.

Focusing on P05 and P06, the design of the micropile reinforcement achieved a global safety factor for the quasi-permanent combination (2.16), which would lead for P06 to a load transfer of

Table 1. Global safety factor SF for pier 1 to 6.

Pier	Safety Factor(1)	Load(2) MN	Load transfer(3) %
P01	1.14	56.1	43
P02	1.00	56.1	50
P03	1.00	56.1	50
P04	1.13	56.1	43
P05	1.54	56.1	29
P06	1.27	56.1	41

(1): Before reinforcement
(2): Abutment load for a quasi-static combination
(3): Load transfer to the micropiles to verify the SLS load capacity of each pillar

41% (= 1–1.27/2.16) of the total pier load to the micropiles – and 29% (= 1–1.54/2.16) for P05. For each pier, 16 micropiles anchored 8 m into the marl are required. A global safety factor of 2.00 was achieved for P01 to P04.

4.2 *Measured load transfer process*

As discussed in Section 3, the HST method provides a reliable assessment of the irreversible settlement of each pier. Then, assuming that each micropile is perfectly sealed to the masonry, the HST model gives the irreversible settlement from the exact day the micropiles were sealed until today. By taking into account the stiffness of the micropile gathered from static loading test, and considering a linear behavior, the load transfer ratio can be accurately calculated (see Table 2).

Table 2. Measured load transfer ratio for pier 1 to 6.

Pier	Settlement(1) mm	$16.K_{\mu p}^{(2)}$ kN/m	Load transfer(3) %	FS(4)
P01	5.1	$1.6 \cdot 10^6$	14	1.33
P02	11.3	$1.6 \cdot 10^6$	32	1.47
P03	12.4	$1.6 \cdot 10^6$	35	1.55
P04	11.6	$1.6 \cdot 10^6$	33	1.69
P05	3.4	$1.6 \cdot 10^6$	10	1.71
P06	6.9	$1.6 \cdot 10^6$	19	1.57

(1): Settlement since the sealing of the micropiles on the masonry
(2): Stiffness of the reinforcement (16 micropiles/pier)
(3): Calculated load transfer ratio between the pier and the micropiles
(4): Factor of safety of the actual bearing capacity of the wood pile group

It appears, especially for the P06 pier, that settlements are stabilized (see Figure 5c), which entails that the load transfer process is about to be completed. The load transfer ratios deduced from settlements are lower than achieved (see Tables 1 and 2). Initially, in the French practice of designing deep foundations according to the pressumeter test, the global safety factor reached for deep foundation is about 2.5 ($= Q_L/Q$ where Q_L is the limit bearing capacity load and Q is the applied load).

When using the static loading test on isolated pile, the acceptable limit load (Q_N) is defined as $0.66 \cdot Q_{cr}$, where Q_{cr} is the creep limit load obtained by a static pile loading test (Baguelin 1970). As the French practice consists on a dual approach (pressumeter and static load test), the application of a load $Q = Q_{cr}$ on a single pile is equivalent to have, for the considered pile, a safety factor SF = 1.66 ($= Q_L/Q_{cr} = 0.66 \cdot 2.5$).

In fact, the stabilization of settlements ($v_1 \leq 0.15$ mm/year) seems to be obtain when the safety factor edges 1.5 to 1.7 for the wood pile group. It appears that the load transfer draws up when the load on the wooden group piles is limited to the creep limit load of the group.

4.3 *Soil-pile-soil interaction approach*

4.3.1 *Elastic behavior*

Settlement of piles group can be treated by the theory of elasticity. The calculations are based on an interaction factor ratio α, defined as the ratio of the additional settlement due to an adjacent pile to the settlement of the pile under its own load. The interaction factor is determined in a configuration of two piles separated by a distance d and considering a pile loaded at the source and a passive unloaded pile undergoing the settlement of the source pile (see Figure 7). The settlement analysis of the pile group is then performed assuming a superposition principle: each pile undergoes the sum of the interactions of all other piles in the group (Poulos 1968). This approach, initially based on the Mindlin equation, was simplified and improved by Mylonakis by considering a Winkler model of soil reaction in a layered soil (Mylonakis 1998).

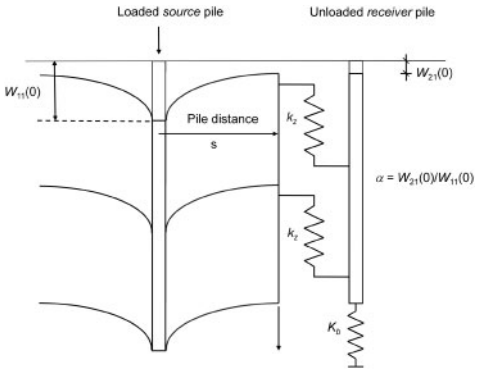

Figure 7. Pile group settlement analysis (Mylonakis).

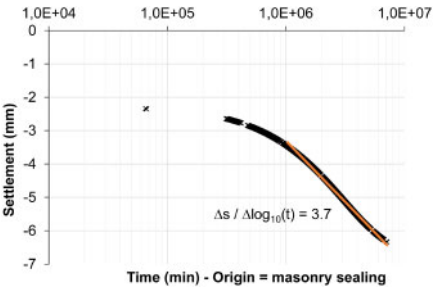

Figure 8. Creep rate of pier P06.

The settlements of loaded source piles and unloaded receiver piles are based on the elasticity theory (Young modulus E and Poisson ratio ν) and the "magical radius" defined by Randolph and Worth (Randolph, 1978) as the distance beyond which soil settlement disappears.

According to the pressumeter theory, the isolated pile settlement is based on the pressumeter modulus E_M (Frank 1982) and transfer functions for the interaction of the shaft and pile tip with the soil, which have been fitted to Young's modulus by a multiplication factor $E = k \cdot E_M$, to ensure the equivalence between the two approaches (Cuira 2016). In our case, choosing the Mylonakis formulation, we obtain $k = 3.6$ for the isolated pile. The settlement of a wood pile in an infinite group of piles is then calculated, the two approaches (Mylonakis and Frank and Zhao – see Table 3) are consistent and give similar results.

Table 3. Pile group settlement.

Pier	$s^{(1)}_{0,M}$ mm	$s^{(2)}_{0,FZ}$ mm	$s^{(3)}_{\infty,M}$ mm	$s^{(4)}_{\infty,FZ}$ mm	$s^{(5)}_{wp,gr}$ mm	$K^{(6)}_{wp,gr}$ kN/m
P05	3.59	–	–	–	27.2	$2.064 \cdot 10^6$
P06	3.53	3.48	40.1	41.6	26.1	$2.176 \cdot 10^6$

(1) Settlement of an isolated wooden pile according to the Mylonakis model
(2) Settlement of an isolated wooden pile according to the Frank & Zhao model
(3) Settlement of a wooden pile in an infinite group according to the Mylonakis model
(4) Settlement of a wooden pile in an infinite group according to the Frank & Zhao model
(5) Settlement of the wooden pile group as a rigid pile cap according to Mylonakis
(6) Stiffness of the wooden pile foundation

Assuming that wood piles are strongly connected to the wooden decking which is equivalent to a rigid pile cap, the settlement and stiffness ($K_{wp,gr}$) of the foundation of the wooden pile cap group can be calculated, all results are shown in Table 3. Before micropile reinforcement, the effect factor of the collective piles of each pile of the 235 wooden piles can be defined as $GE = s_{wp,gr}/s_{0,M}$. This factor is equal to 7.39 for P06.

After reinforcement, the settlements of the piers and then the group effect of the piles are reduced. Assuming elastic behaviour, the group effect factor after strengthening is calculated as follows:

$$GE_{reinf} = \left(K_{wp,gr} / \left(K_{wp,gr} + 16 \cdot K_{\mu p}\right)\right) \cdot GE$$

For P06, we obtain $GE_{reinf} = 4.25$. Numerous static load tests performed on the piles showed that the creep limit load corresponds to a creep rate (settlement per logarithmic time unit) of

1.5 mm/$\log_{10}(t)$ (t in minute). The settlement of the P06 pile after strengthening is shown in Figure 8. The creep rate, equal to 3.7 mm/$\log_{10}(t)$, is evaluated on the linear part of the curves. Application of the group effect factor leads to a creep rate value of 0.9 mm/$\log_{10}(t)$ for an isolated pile, just below the creep limit load rate. The result is consistent with the safety factor deduced from the measured load transfer.

4.3.2 *Visco-elastic behavior*

Analysis of tidal effects on pile settlements

Assuming that the load on the foundation of the wood pile group is directly related to buoyancy, the tidal effects can be analyzed in terms of settlements. Figure 9 shows the measured settlements and calculated settlements for P06 assuming elastic behaviour of the wood pile group foundation (stiffness $K_{wp,gr}$). It appears that bridge settlements are strongly damped compared to the results of elasticity theory. The damping parameter can be adjusted by assuming that the foundation acts as a Kelvin-Voigt element defined by the stiffness $K_{wp,gr}$ and the damping $C_{wp,gr}$ (see Figures 11 and 10). The lag time between measured settlement curve and tide is about 3 hours.

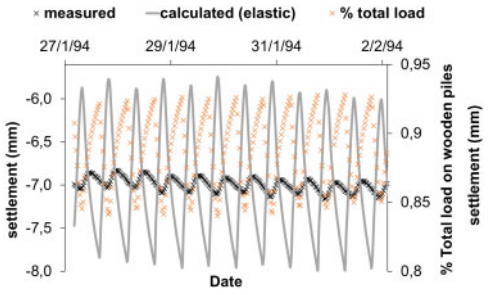

Figure 9. Measured and calculated tidal settlements.

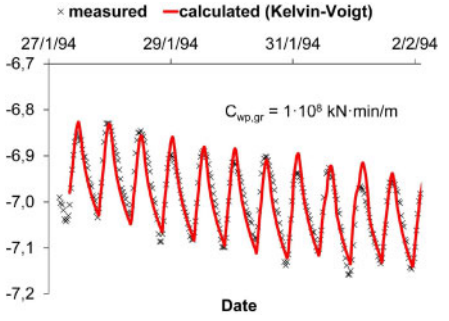

Figure 10. Fitted Kelvin-Voigt model.

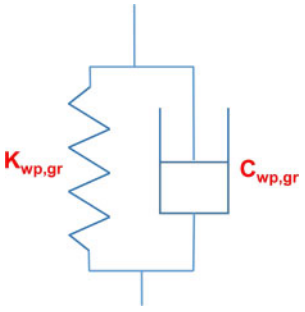

Figure 11. Kelvin-Voigt element model.

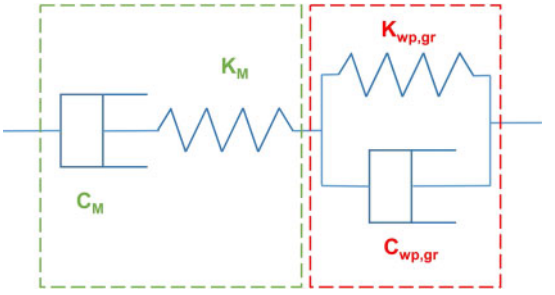

Figure 12. Burgers model of pier foundation.

Analysis of pier settlements by creep

Creep settlement analysis of pile foundations can be handled by viscoelastic theory, usually with a logarithmic creep rate function (Booker 1976; Cambefort 1965). As shown in the HST analysis, the creep rate before reinforcement is a linear function of time (Figure 4-c). Piers foundations can be modelled by a Burgers element (series of Kelvin-Voigt and Maxwell elements) as shown in Figure 12. Assuming infinite stiffness K_M, the damping parameter C_M is directly given by the HST method and $C_M = 9.228 \cdot 10^{12}$ kN·min·m^{-1}. For consistency, we check that $C_M \gg C_{wp,gr}$.

Analysis of wooden pile group by creep

In order to account for linear creep, the Mylonakis formulation could be adapted by replacing the Wrinkler springs with Burgers elements as shown in Figure 13.

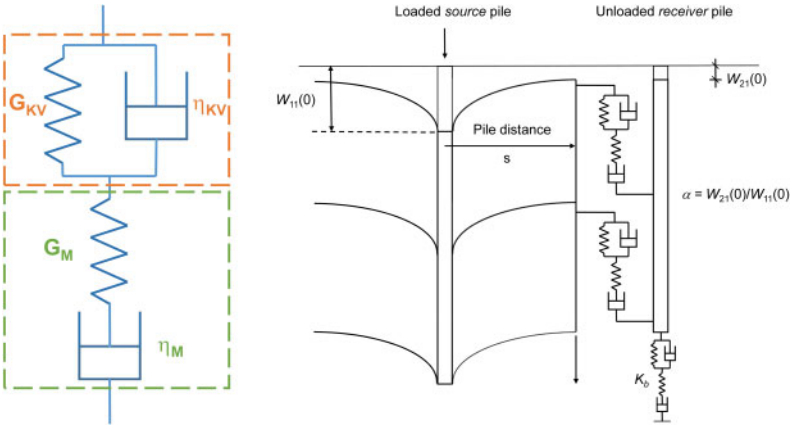

Figure 13. Principle of creep settlement analysis of pile groups (modified Mylonakis).

For each soil layer, the shear modulus G_{KV} are defined according to the theories of elasticity and pressumeters (see 4.3.1), and G_M is choosen as infinite because it has no consequence on measured creep settlements. The damping parameter η_{KV} and η_M of clay are defined according to the bibliography for similar soils tested (Guo 2000), in particular, for clay, $\eta_{KV} = 0.48 \cdot G_{KV} \cdot (10^5 \text{s})$. This latter value fits well with tidal settlements (Figure 15).

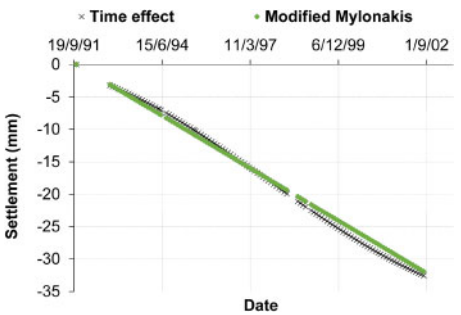

Figure 14. Modelled creep settlement (η_M fitting).

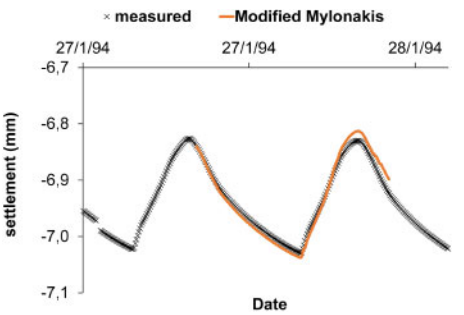

Figure 15. Modelled tidal settlement (η_{KV} fitting).

For silty sand, η_{KV} has negligible influence on tidal settlements, and η_M, which is the most influential long-term creep parameter and is fitted to pier settlements by creep (Figure 14). All properties are listed in Table 4.

Table 4. Burgers parameters for the whole foundation and for soil – pile transfer function.

Layer	G_{KV} MPa	G_M MPa	η_{KV} MPa·day	η_M MPa·day	$K_{wp,gr}$ kN·m^{-1}	$C_{wp,gr}$ kN·min·m^{-1}	K_M kN·m^{-1}	C_M kN·min·m^{-1}
Clay	4.196	∞	2.347	$2.0 \cdot 10^3$	$2.176 \cdot 10^6$	$1.0 \cdot 10^8$	∞	$9.228 \cdot 10^{12}$
Silty sand	20.770	∞	55.55	$1.17 \cdot 10^5$				

The results are consistent with the behavior of a group of piles: for low stress and low strain (tidal effects) only the shaft friction is mobilized and for high stress and high strain, the tip of the pile is mainly mobilized (long term creep).

4.3.3 *Analysis of the effects of micropiles on creep settlements*

Using the Burgers macro-element

Based on the measurement analysis and the pile-soil-pile interaction, the properties of the Burgers equivalent element of the pier foundation were defined in the previous paragraphs. The sealing of the micropiles to the structure is, in this model, equivalent to adding a spring in parallel to the Burgers element (Figure 16).

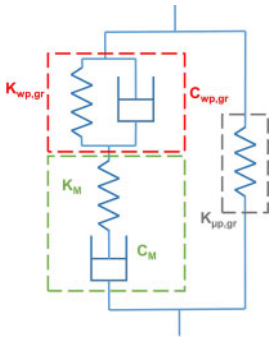

Figure 16. Modelled micropiles reinforcement.

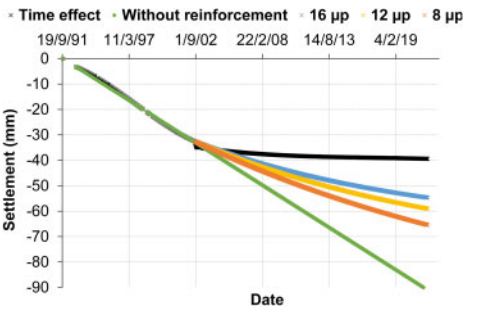

Figure 17. Wooden piles unloading process for P06.

Using Boltzmann's principle and considering that the unloading of the wooden foundation piles onto the micropiles is equivalent to a stress relaxation of the Burgers element, the settlements of the pier after the micropiles have been sealed can be calculated by an iterative process (the unloading increment dq at $t+dt$ depends on the settlement at t, estimated by $dq = K_{\mu p,gr}\ s(t)$). The unloading process is mainly determined by the Maxwell creep parameters of the wood pile foundation and the stiffness of the micropiles. It is possible to test several reinforcement hypotheses (8, 12, 16 micropiles/pier, Figure 17). It seems that the model overestimates settlements, which could be explained by the evolution of the creep parameters of the wood pile foundation due to their unloading (not taken into account in this model).

Using modified Mylonakis model (viscoelasticity)

The Mylonakis model can be adapted in order to integrate micropiles, settlements after reinforcement can also be calculated with an acceptable accuracy (see Figure 18). Different hypotheses are

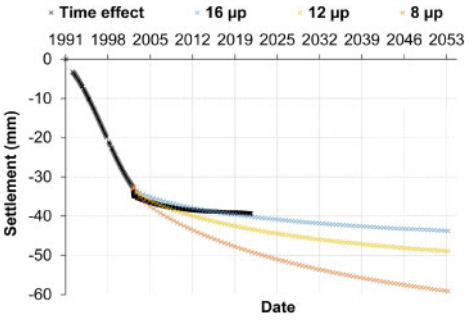

Figure 18. Calculated and measured settlements.

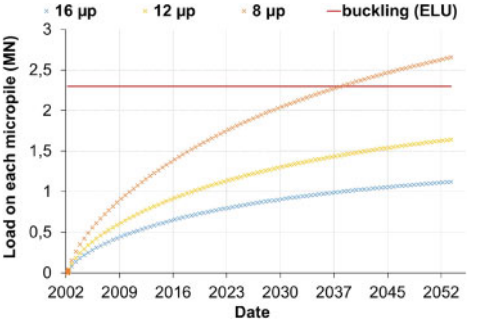

Figure 19. Load transfer and resistance.

tested, it is shown that the buckling resistance (which is the design case) of each micropile is overpassed in the 8 micropiles/pier hypothesis, the initial design (reinforcement by 16 micropiles/pier) is confirmed.

5 CONCLUSION

The article discusses the importance of analyzing monitoring results, especially for sensitive structures such as the Pont de Pierre. To be consistent, the analysis must be performed with appropriate methods. In this case, the HST method provides reversible and irreversible components of the measurements and a convincing explanation of the structure's behavior in relation to creep and tidal and seasonal effects. Associated with analytical models of group piles foundations, pile – soil – pile and soil – structure interactions relevant analysis of settlements and effects of micropiles on the structure can be performed. The Mylonakis pile group model is adapted to incorporate the viscoelastic behavior of the foundation. Two scales are to be considered: a global scale, consistent for the design of the stiffness of the micropiles, and a local scale, adapted to the analysis of each wooden pile and micropile and its interaction with the structure in order to evaluate the pinching effect on the masonry. The approach could be improved by coupling a thermal model to evaluate, based on seasonal effects, the evolution of damping parameters with time.

REFERENCES

Baguelin F., Jezequel J., Marchal J. 1970. Essai statique de fondations profondes, *Bulletin de Liaison des Laboratoires Routiers* 44(2):161–177

Bonelli S. 2008. On pore-pressure analysis in earthdams. *International Water Power and Dam Construction* 60(12):36–39.

Bonelli S. 2009. Approximate solution to the diffusion equation and its application to seepage-related problems. *Applied Mathematical Modelling* 33(1):110–126.

Booker J.R., Poulos H.G. 1976. Analysis of creep settlement of pile foundations, *Journal of Geotechical Engineering Division* 102(1):1–14.

Cambefort H., Chadeisson R. 1965. Critère pour l'évaluation de la force portante d'un pieu, Compte-Rendu du 6ème *Congrès International de Mécanique des Sols et des Travaux de Fondations*, Montréal.

Carrère A., Colson M., Goguel B., Noret C. 2000. Modelling: a means of assisting interpretation of readings. *Proc. XXth International Congress on Large Dams*, Beijing, ICOLD, p. 1005–1037.

Christin J., Reiffsteck P., Le Kouby A., 2013. Projet Pieux Bois.

Cuira F., Flavigny E. 2016. Essai pressiométrique et calculs par éléments finis, 5ème *Congrès Maghrébin en Ingéniérie Géotechnique*, Marrakech.

Ferry S., Willm G. 1958 Méthodes d'analyse et de surveillance des déplacements observés par le moyen de pendules dans les barrages. *Proc.VIth International Congress on Large Dams*, New-York, ICOLD, p. 1179–1200.

Forbes J.D. 1846. Account of some experiments on the temperature of the earth at different depths and in different soils near Edinburgh. *Transactions of The Royal Society of Edinburgh* 16:189–236.

Frank R., Zhao S. 1982. Estimation par les paramètres pressiométriques de l'enfoncement sous charge axiale de pieux forés dans les sols fins, *Bulletin de liaison des ponts et chaussées* 199:17–24.

Guedes Q.M., Coelho P.S.M. 1985. Statistical behaviour model of dams. *Proc. XVth International Congress on Large Dams*, Lausanne, ICOLD, p. 319–334.

Guo W.D., 2000. Visco-elastic transfer models for axially loaded piles, *International Journal for Numerical and Analytical Methods in Geomechanics* 24, 135–163.

Mylonakis G., Gazetas G. 1998. Settlement and additional internal forces of grouped piles in layered soil, *Géotechnique* 48(1):55–72.

NF P94-262. 2012. Justification des Ouvrages Géotechnique, Fondations profondes.

Poulos H.G. 1968. Analysis of the settlement of pile groups, *Géotechnique*, 18:449–471.

Randolph M.F., Worth C.P., 1978 Analysis of deformation of vertically loaded pile, *Journal of Geotechnical Engineering, ASCE* 104(12):1465–1488.

Young P. 1998. Data-based mechanistic modelling of environmental, ecological, economic and engineering systems. *Environmental Modelling & Software* 13:105–122.